Supporting Information

Benzo-Fused Periacenes or Double Helicenes? Different Cyclodehydrogenation Pathways on Surface and in Solution

Qigang Zhong,[1,2,#] Yunbin Hu,[3,4,#] Kaifeng Niu,[1] Haiming Zhang,[1] Biao Yang,[1] Daniel Ebeling,[2] Jalmar Tschakert,[2] Tao Cheng,[1] André Schirmeisen,[2] Akimitsu Narita,[3,5] Klaus Müllen,[3,6*] Lifeng Chi[1*]*

(1) Institute of Functional Nano & Soft Materials (FUNSOM), Jiangsu Key Laboratory for Carbon-Based Functional Materials and Devices, Soochow University, Suzhou 215123, China

(2) Institute of Applied Physics, Justus-Liebig University, Heinrich-Buff-Ring 16, 35392 Giessen, Germany

(3) Max Planck Institute for Polymer Research, 55128 Mainz, Germany

(4) Department of Organic and Polymer Chemistry, College of Chemistry and Chemical Engineering, Central South University, Changsha, Hunan 410083, China

(5) Organic and Carbon Nanomaterials Unit, Okinawa Institute of Science and Technology Graduate University, Okinawa 904-0495, Japan

(6) Institute of Physical Chemistry, Johannes Gutenberg University Mainz, Duesbergweg 10-14, 55128 Mainz, Germany

[#]These authors contributed equally.

Table of Contents

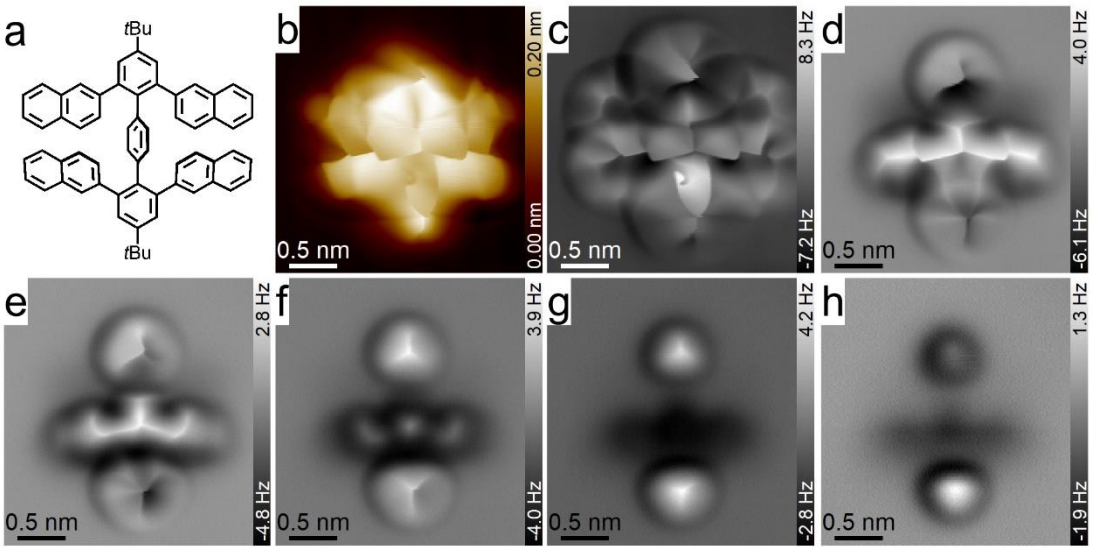

Figure S1. Intact TNTP-*t*Bu **1a** on Cu(110). (a) Chemical structure of TNTP-*t*Bu **1a**; (b) High-resolution STM image of an individual TNTP-*t*Bu **1a** molecule adsorbed on Cu(110); (c) Frequency shift AFM image of the same molecule recorded in constant-current mode; and (d-h) Constant-height frequency shift AFM images of this molecule at different tip-heights. Imaging parameters: (b,c) 10 mV, 100 pA; Tip heights Z = 0 pm (d), +50 pm (e), +100 pm (f), +150 pm (g) and +200 pm (h), where the + signs represent an increase of the tip-sample distance relative to an STM set point (0.1 V, 10 pA) on the adjacent Cu(110) surfaces.

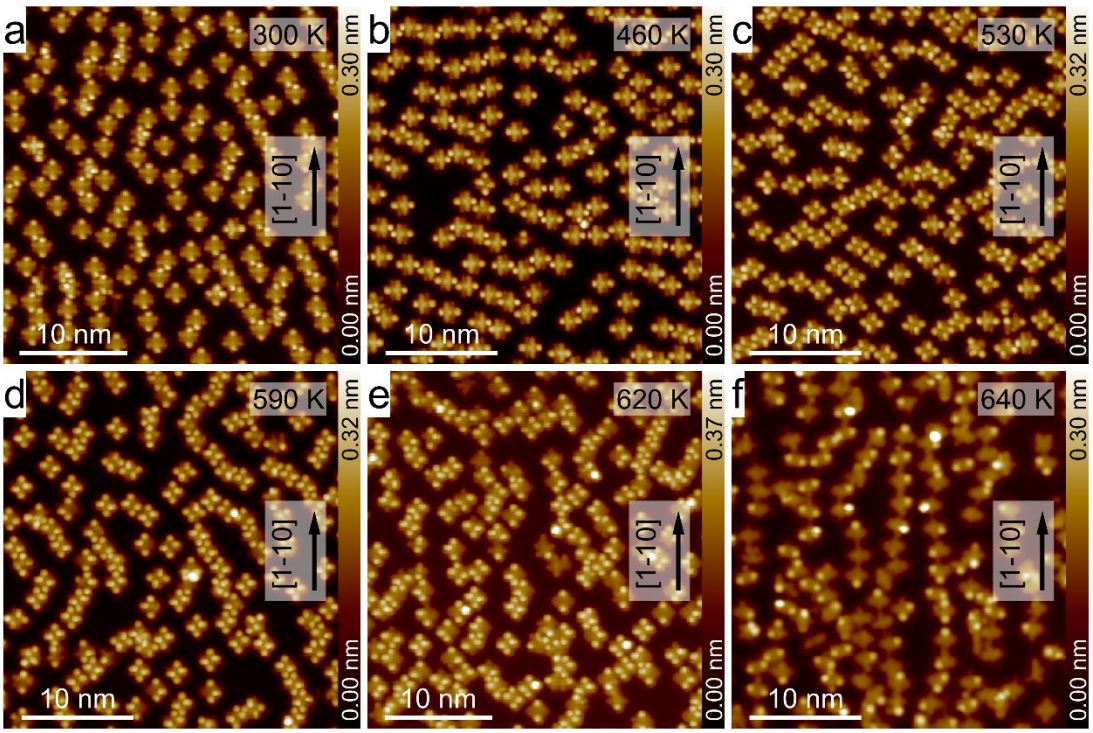

Figure S2. STM overviews of the annealed TNTP-*t*Bu/Cu(110) samples. (a-f) STM images taken after 30 min annealing at 300 K (100 min), 460 K, 530 K, 590 K, 620 K and 640 K, respectively. Imaging parameters: (a-f) 0.1 V, 10 pA.

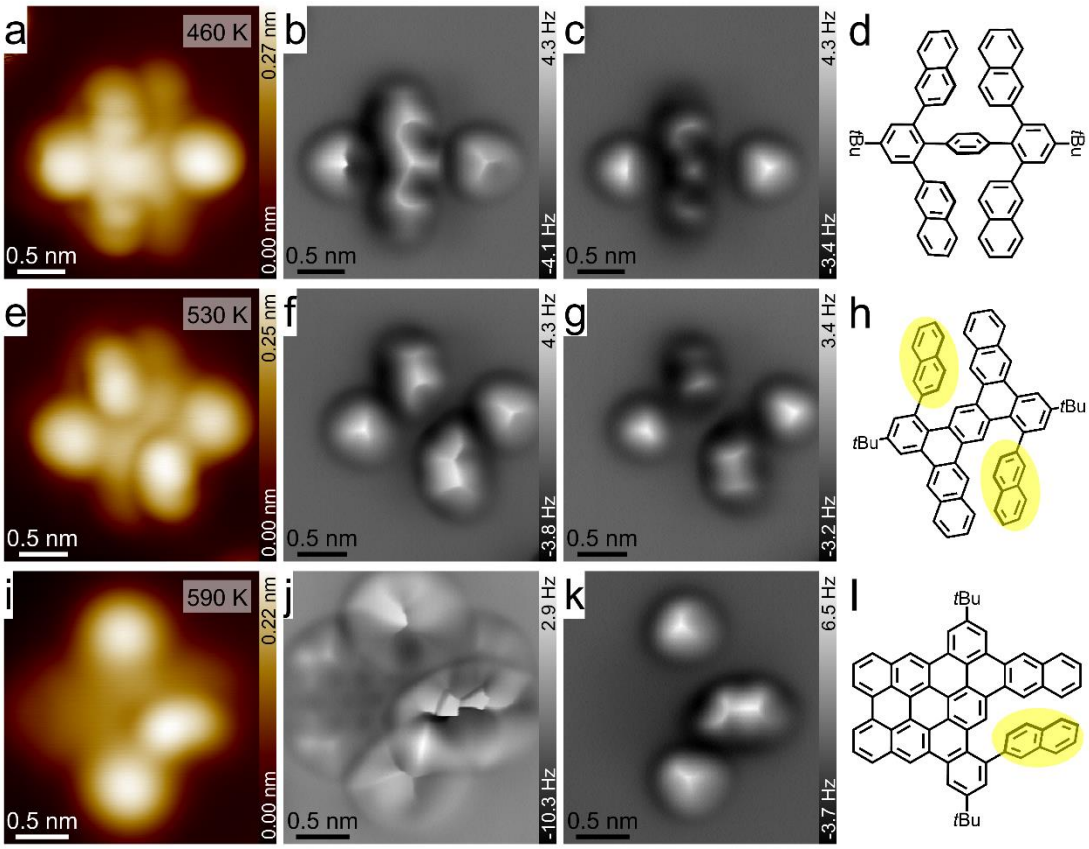

Figure S3. Unimolecular images of the intact and intermediate states of TNTP-*t*Bu **1a** on Cu(110). (a) STM image of an individual TNTP-*t*Bu molecule **1a** taken after annealing the TNTP-*t*Bu/Cu(110) sample at 460 K; (b,c) Constant-height AFM images of this molecule; (d) The corresponding chemical structure; (e) STM image of a single intermediate molecule taken after annealing at 530 K; (f,g) Corresponding constant-height AFM images; (h) The chemical structure of this intermediate, where the steric naphthyl groups are marked with yellow ovals; (i) STM images of the half planarized intermediate; (j) Frequency shift AFM image of the intermediate molecule that was obtained with constant-current feedback and a CO-functionalized tip; (k) Constant-height AFM image of this intermediate; and (l) The corresponding chemical structure, where the steric naphthyl group is marked with a yellow oval. Imaging parameters: (a,e) 0.1 V, 10 pA; (i,j) 10 mV, 100 pA; Tip heights Z = 50 pm (b), +100 pm (c), +50 pm (f), +100 pm (g) and +100 pm (k), where the + signs represent an increase of the tip-sample distance relative to an STM set point (0.1 V, 10 pA) on the adjacent Cu(110) surfaces.

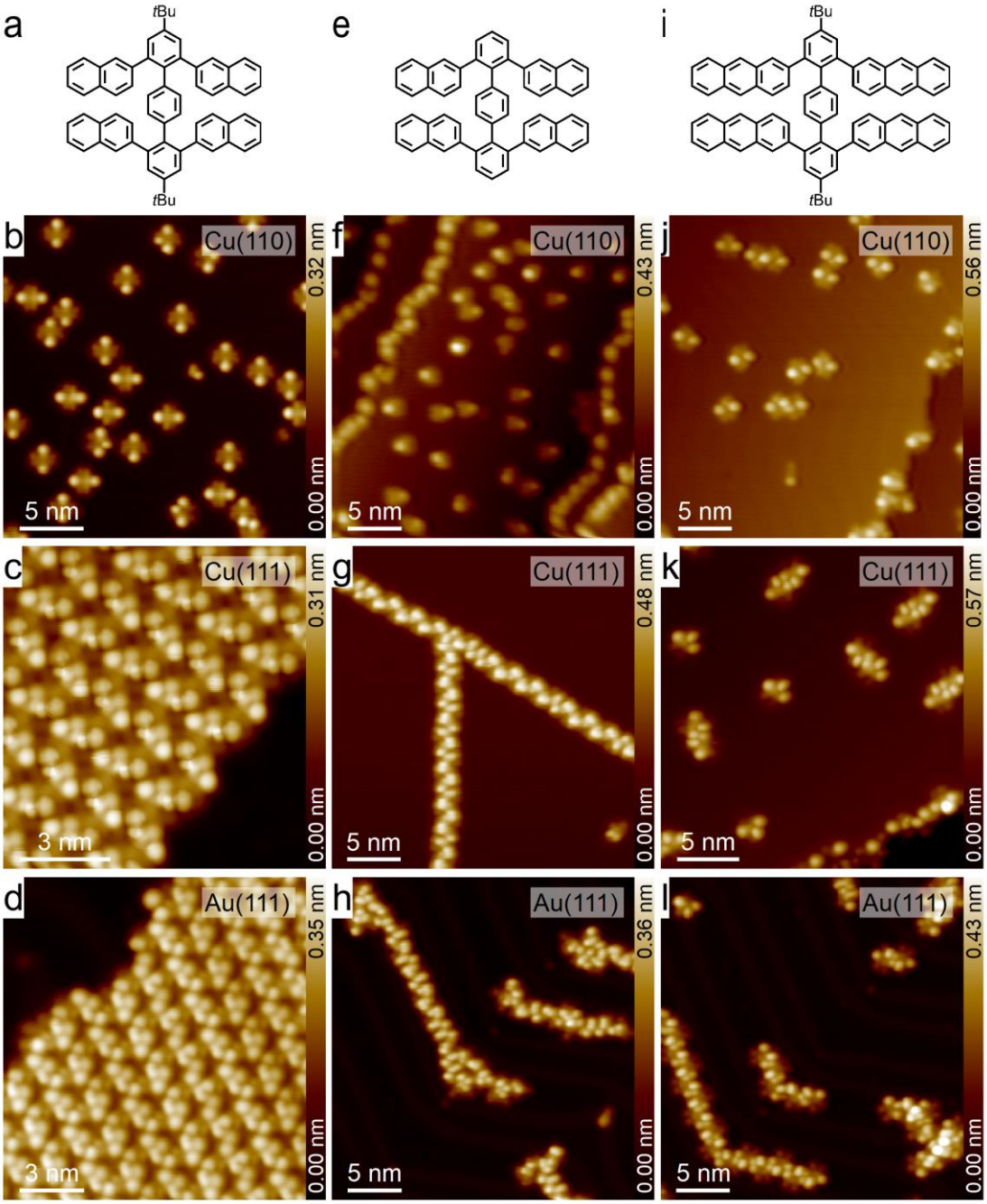

Figure S4. STM overviews of intact TNTP-*t*Bu **1a**, TNTP **1b** and TATP-*t*Bu **5** that were adsorbed on Cu(110), Cu(111) and Au(111), respectively. (a,e,i) Chemical structures of TNTP-*t*Bu **1a**, TNTP **1b** and TATP-*t*Bu **5**, respectively; (b-d) STM images of the TNTP-*t*Bu **1a** decorated Cu(110) (b), Cu(111) (c) and Au(111) (d) samples; (f-h) STM images of the TNTP **1b** decorated Cu(110) (f), Cu(111) (g) and Au(111) (h) samples; and (j-l) STM images of the TATP-*t*Bu **5** decorated Cu(110) (j), Cu(111) (k) and Au(111) (l) samples. Imaging parameters: (b,d,k) -1.0 V, 100 pA; (c) 0.1 V, 10 pA; and (f,g,h,j,l) -1.0 V, 10 pA.

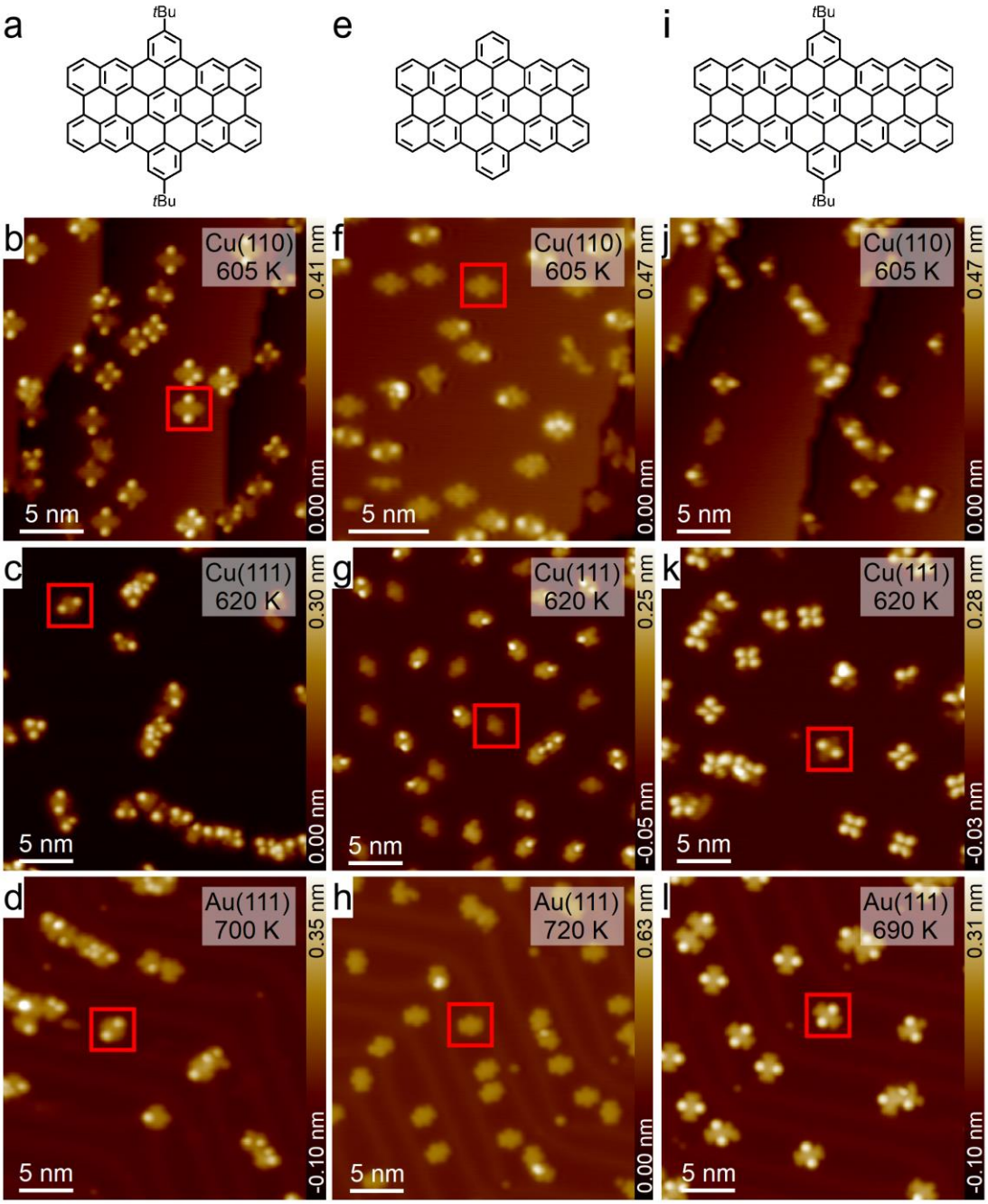

Figure S5. STM overviews of the annealed TNTP-*t*Bu/M, TNTP/M and TATP-*t*Bu/M samples (M = Cu(110), Cu(111) or Au(111)). (a,e,i) Chemical structures of dibenzoperihexacene **3a**, dibenzoperihexacene **3b** and dibenzoperioctacene **6**, respectively; (b-d) STM images of dibenzoperihexacene **3a** decorated Cu(110) (b), Cu(111) (c) and Au(111) (d) samples; (f-h) STM images of dibenzoperihexacene **3b** decorated Cu(110) (f), Cu(111) (g) and Au(111) (h) samples, where the yield of intact **3b** are 32% (8/25), 30% (9/30) and 56% (15/27) on Cu(110), Cu(111) and Au(111), respectively; and (j-l) STM images of dibenzoperioctacene **6** decorated Cu(110) (j), Cu(111) (k) and Au(111) (l) samples. A dibenzoperihexacene/dibenzoperioctacene molecule is marked with a red box as an example on each image when it can be found. Imaging parameters: (b) -0.1 V, 1.0 nA; (c,f,g) -1.0 V, 100 pA; (d,h,j,k) -1.0 V, 10 pA; and (l) -1.0 V, 5 pA.

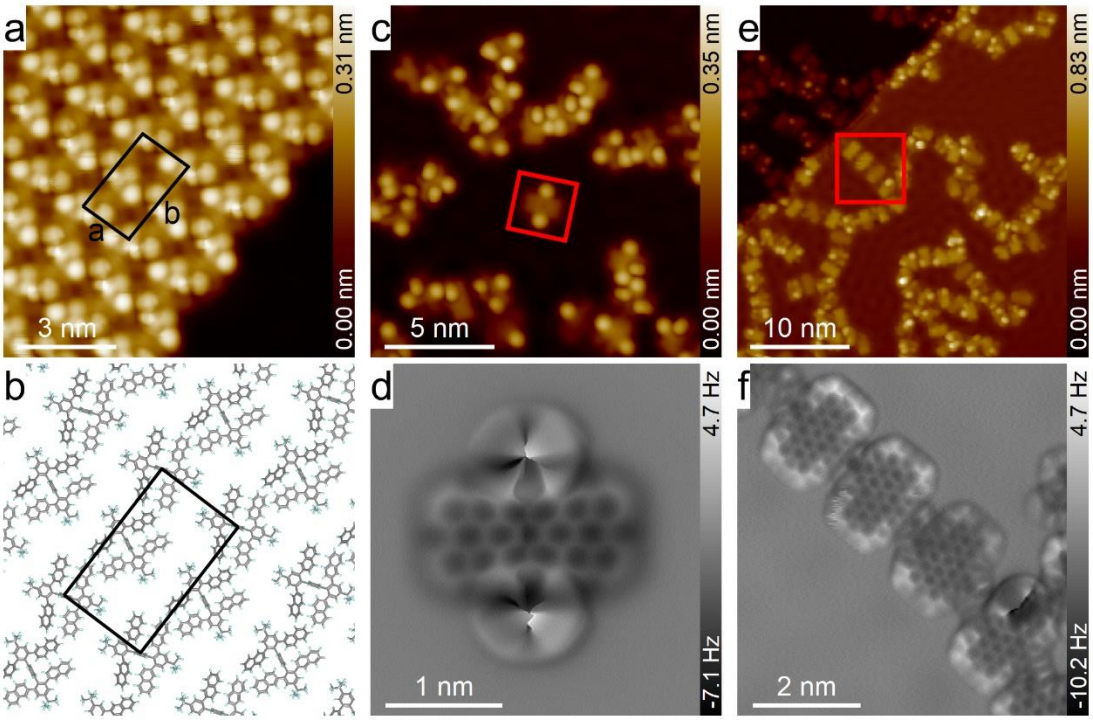

Figure S6. Cyclodehydrogenation reactions of TNTP-*t*Bu **1a** on Cu(111). (a) STM overview of the self-assembly of the TNTP-*t*Bu **1a** molecules. (b) Corresponding assembly model, where the unit cell of the self-assembly is marked with black boxes in (a,b), and the orthogonal primitive vectors ***a*** and ***b*** are 2.87 nm and 1.72 nm, respectively, in length. (c) STM overview of the TNTP-*t*Bu/Cu(111) sample after annealing at 620 K for 30 min; (d) Constant-height AFM image of a single planarized product marked with a red dashed square in (c); (e) STM overview of the TNTP-*t*Bu/Cu(111) sample after annealing at 630 K for 30 min; and (f) Constant-current frequency shift AFM image of a linked product chain marked in (e) with a red box. Imaging parameters: (a,c,e) 0.1 V, 10 pA; (f) 10 mV, 100 pA; and (d) tip height Z = -80 pm, where the - sign means the decrease of the tip-sample distance relative to the STM set point (0.1 V, 10 pA) on the adjacent Cu(111) surfaces.

Table S1. The rotation barrier (in eV) of a naphthyl group of **1a** on the bond connected to the terphenyl base in solution, on the Au(111) surface and the Cu(110) surface, and the adsorption energy of **1a** on Au(111) and Cu(110) that is estimated from the reactive force field.

	Solution	Au(111)	Cu(110)
Rotation Barrier (eV)	0.32	0.44	0.46
Adsorption Energy (eV)	-	-	-2.48

We conducted reactive force field simulations to estimate the rotation barrier of 1a at different conditions. The rotation barrier of a naphthyl group of **1a** is 0.32 eV in solution. On Au(111), the rotation barrier is 0.44 eV, which is 0.12 eV higher than that of the solution. On Cu(110), the rotation barrier is 0.46 eV, which is 0.14 eV higher that of the solution. Thus, the presence of a metal substrate increases the rotation barrier, thereby making the rotation on the surfaces more difficult.

We also estimated the adsorption energy of 3a on Au(111) and Cu(110), which is defined as follows:

$$\Delta E = E_{\text{total}} - (E_{\text{1a}} + E_{\text{surface}}) \quad \text{(S1)}$$

Table S2. Adsorption energies (ΔE_a, in eV) of **3a** and **2a-1** on Cu(110) from DFT calculations.

Structure	Adsorption energy (eV)
3a	-8.79
2a-1	-4.14

We estimated the relative stability by calculating the adsorption energy (ΔE_a) of **3a** and **2a-1** from DFT calculations, as follows:

$$\Delta E_a = E_{sur+ads} - (E_{sur} + E_{ads}) \quad (2)$$

Here, $E_{sur+ads}$ is the energy of surface with an adsorbent, E_{sur} is the energy of metal slab and E_{ads} is the energy of isolated adsorbent. Our DFT calculations show that ΔE_a of **3a** is -8.79 eV, ΔE_a of **2a-1** is -4.14 eV, as shown in Table S2., which indicates that the metal surface prefers to stabilize the flatten structure (**3a** with larger binding energy) than jagged structure (**2a-1**). We consider these DFT calculations provide evidence to explain the experimentally observed different trends in selectivity between solution reaction and metal surface catalyzed reaction.

Spin density of the radical cation species of precursor **1b** was calculated by DFT at the UB3LYP/6-31G (d,p) level of theory, using the Gaussian 09 software package.[3] The higher spin density at the α-position over the β-position of the naphthyl moiety explains the regioselectivity of the oxidative cyclodehydrogenation in solution.

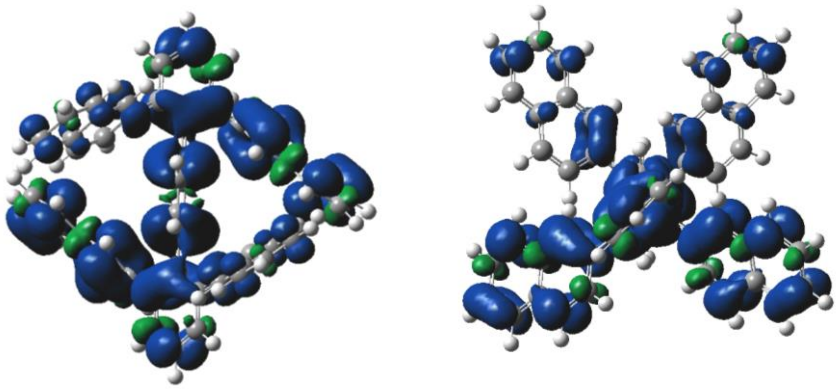

Figure S7. Top and side view of the spin density of **1b** radical cation.

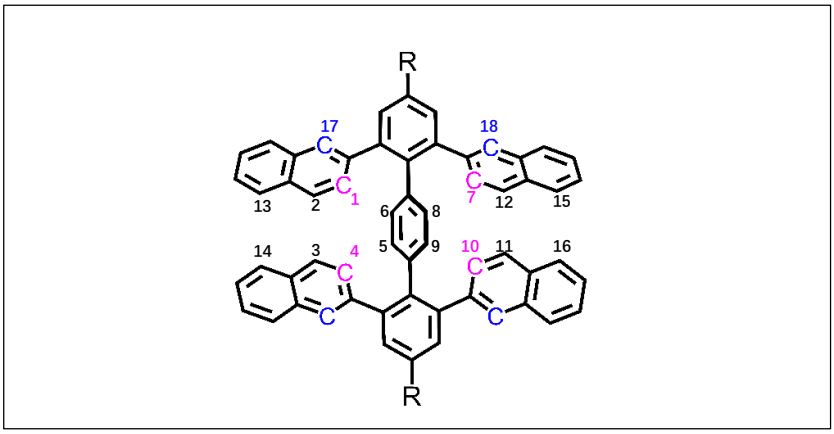

Figure S8 Proposed the reaction processes. The reactions may start from C_1-C_6 and C_9-C_{10} coupling as shown in Figure 2 (structure 1a to structure 4). At 620 K, structure 4 (shown in Fig. 2) directly transforms into structure 3a, which indicates that no stable intermediate exists between structure 4 and structure 3a at this temperature. No other intermediate structure was found, indicating that the planarization of each naphthyl group from structure 4 was accompanied by subsequent or simultaneous formation of three C-C bonds, e.g., C_4-C_5. C_2-C_3 and C_{13}-C_{14}, leading to structure S1, and then to the final product structure 3a.

General Methods

All starting materials were purchased from Aldrich, Acros, and Alfa Aesar and were used as received. Preparative column chromatography was performed using silica gel from Merck with a grain size of 0.063–0.200 mm (silica gel). NMR spectra were recorded in CD_2Cl_2 on AVANCE 300 MHz or AVANCE 500 MHz Bruker spectrometers. Abbreviations: s = singlet, d = doublet, t = triplet, and m = muliplet. High-resolution mass spectrometry (HRMS) was performed on a SYNAPT G2 Si high resolution time-of-flight mass spectrometer (Waters Corp., Manchester, UK) using matrix-assisted laser desorption/ionization (MALDI).

Synthesis

2,2',2",2'"-(4,4"-di-tert-butyl-[1,1':4',1"-terphenyl]-2,2",6,6"-tetrayl)tetranaphthalene (**1a**)[1], 2,2",6,6"-tetrabromo-1,1':4',1"-terphenyl (**7**)[2], and 2,2",6,6"-tetrabromo-4,4"-di- tert-butyl-1,1':4',1"-terphenyl (**8**)[1] were prepared according to the literature.

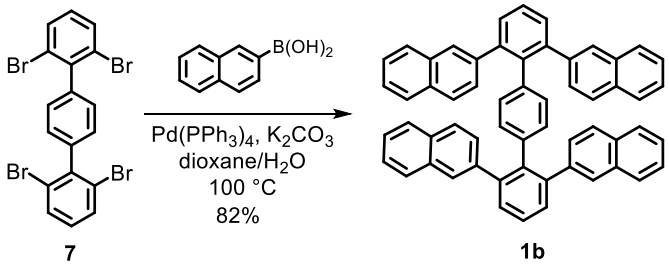

Scheme S1. Synthesis of 2,2",6,6"-tetra(naphthalen-2-yl)-1,1':4',1"-terphenyl (**1b**).

2,2",6,6"-tetra(naphthalen-2-yl)-1,1':4',1"-terphenyl (1b): Under an argon atmosphere, 2,2",6,6"-tetrabromo-1,1':4',1"-terphenyl (**7**) (100 mg, 0.183 mmol), 2-naphthalenylboronic acid (189 mg, 1.10 mmol), $Pd(PPh_3)_4$ (26.4 mg, 0.0229 mmol), and potassium carbonate (291 mg, 2.10 mmol) were dissolved in a degassed solvent mixture of dioxane (5 mL) and H_2O (0.75 mL). The resulting solution was heated to 100 ºC and stirred overnight. After being cooled to room temperature, the reaction mixture was poured into water and extracted using dichloromethane. The organic phase was dried over Na_2SO_4 and evaporated to dryness. The residue was purified via column chromatography with hexane as the eluent and **1b** was obtained as a white powder (110 mg, 82% yield). ^{1}H NMR (300 MHz, CD_2Cl_2, 298 K, ppm) δ

7.86–7.69 (m, 12H), 7.57–7.43 (m, 14H), 7.14 (d, J = 8.5 Hz, 4H), 6.83 (dd, J = 8.5, 1.8 Hz, 4H), 6.62 (s, 4H); ^{13}C NMR (75 MHz, CD2Cl2, 298 K, ppm) δ 142.19, 140.38, 138.67, 137.25, 133.69, 132.28, 131.39, 130.88, 128.80, 128.73, 128.25, 127.91, 127.67, 126.63, 126.30, 126.13. HRMS (MALDI-TOF) *m/z*: Calcd for $C_{58}H_{38}$: 734.2974; Found: 734.3013 (M^+)

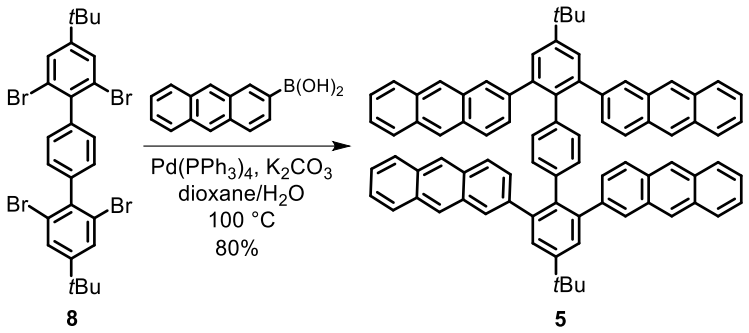

Scheme S2. Synthesis of 2,2',2",2"'-(4,4"-di-tert-butyl-[1,1':4',1"-terphenyl]-2,2",6,6"-tetrayl)tetraanthracene (**5**).

2,2',2",2"'-(4,4"-di-*tert*-butyl-[1,1':4',1"-terphenyl]-2,2",6,6"-tetrayl)tetraanthracene (**5**): Under an argon atmosphere, 2,2",6,6"-tetrabromo-4,4"-di- tert-butyl-1,1':4',1"-terphenyl (**8**) (50 mg, 0.076 mmol), 2-anthracenylboronic acid (138 mg, 0.622 mmol), $Pd(PPh_3)_4$ (11 mg, 9.5 μmol), and potassium carbonate (162 mg, 1.17 mmol) were dissolved in a degassed solvent mixture of dioxane (5 mL) and H_2O (0.75 mL). The resulting solution was heated to 100 ºC and stirred for 24 h. After being cooled to a room temperature, the reaction mixture was poured into water and then filtered. The collected solid was subjected to column chromatography with hot chloroform as the eluent. The crude product was washed with dichloromethane and dried under a vacuum, resulting in compound **5** as a white powder (52 mg, 65% yield). ^{1}H NMR (500 MHz, $C_2D_2Cl_4$, 413 K, ppm) δ 8.35 (s, 4H), 8.06–7.98 (m, 8H), 7.92 (d, J = 8.0 Hz, 4H), 7.87 (s, 4H), 7.50–7.45 (m, 12H), 7.23 (d, J = 8.7 Hz, 4H), 6.84 (d, J = 8.8 Hz, 4H), 6.66 (s, 4H), 1.42 (s, 18H); HRMS (MALDI-TOF) *m/z*: Calcd for $C_{82}H_{62}$: 1046.4852; Found: 1046.4825 (M^+). ^{13}C NMR could not be recorded due to low solubility of **5**.

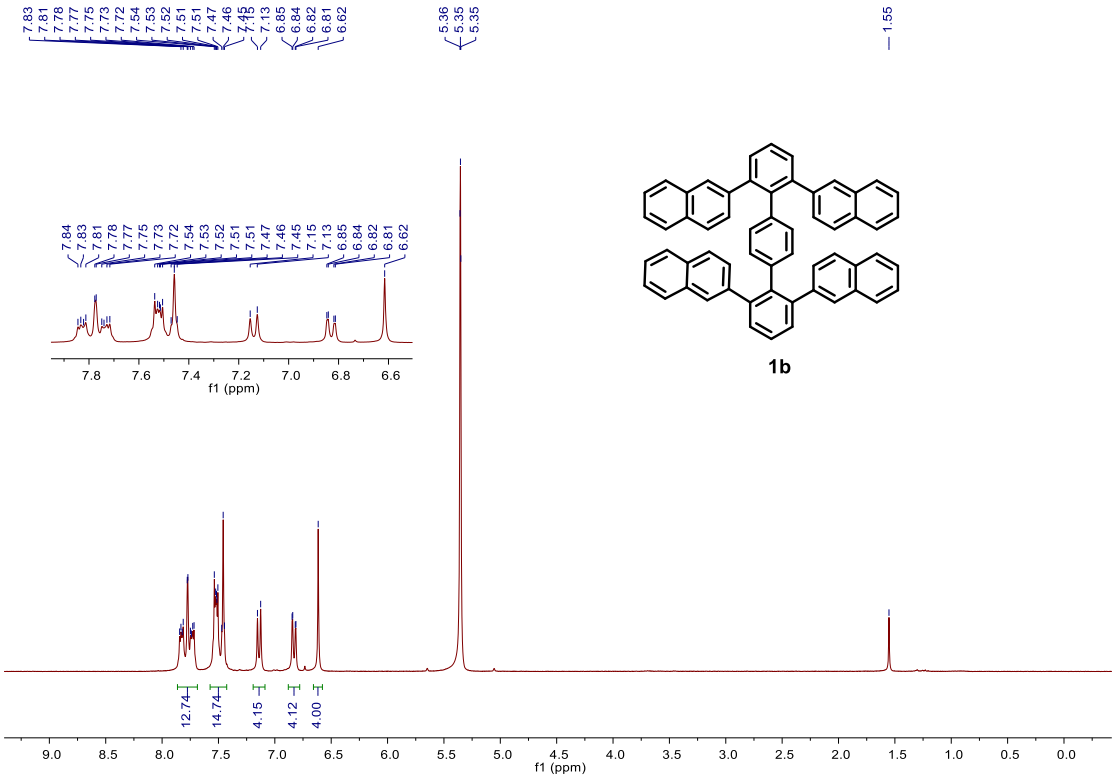

Figure S9. ^{1}H NMR spectrum of **1b** (300 MHz, CD_2Cl_2, 298K).

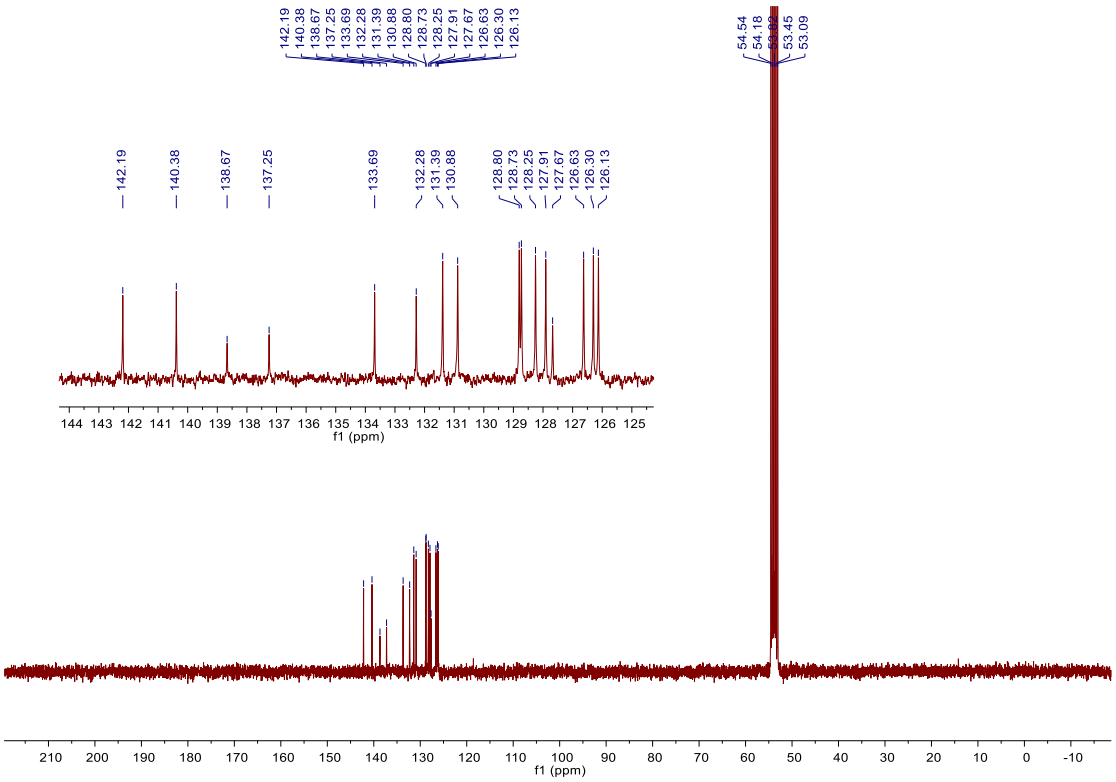

Figure S10. ^{13}C NMR spectrum of **1b** (75 MHz, CD_2Cl_2, 298K).

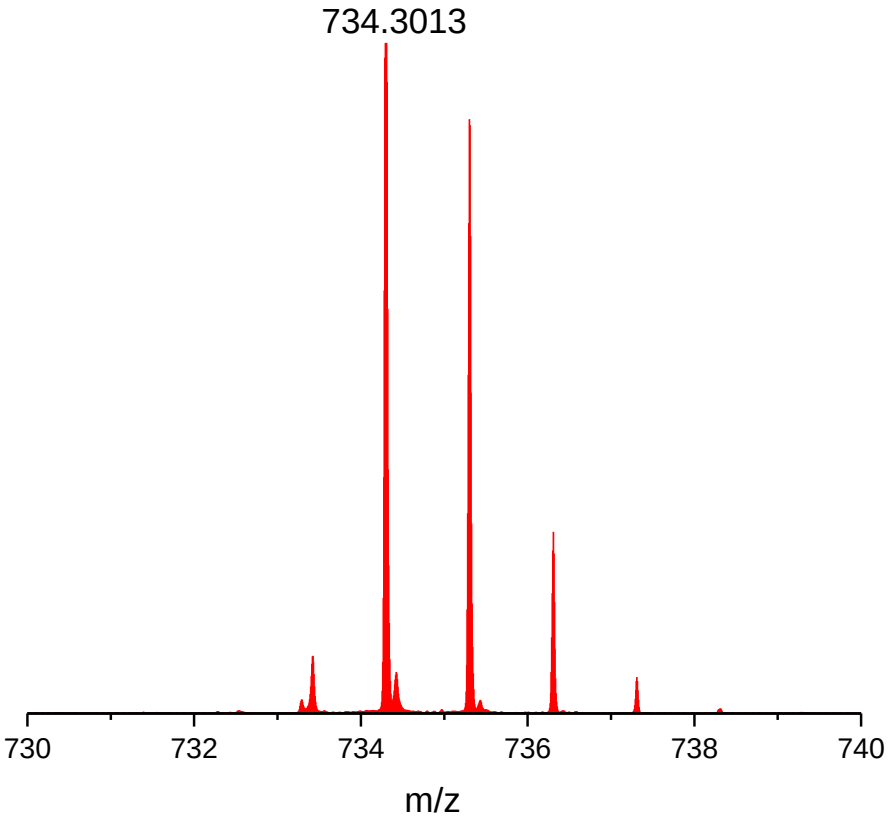

Figure S11. HRMS (MALDI-TOF) spectrum of **1b**.

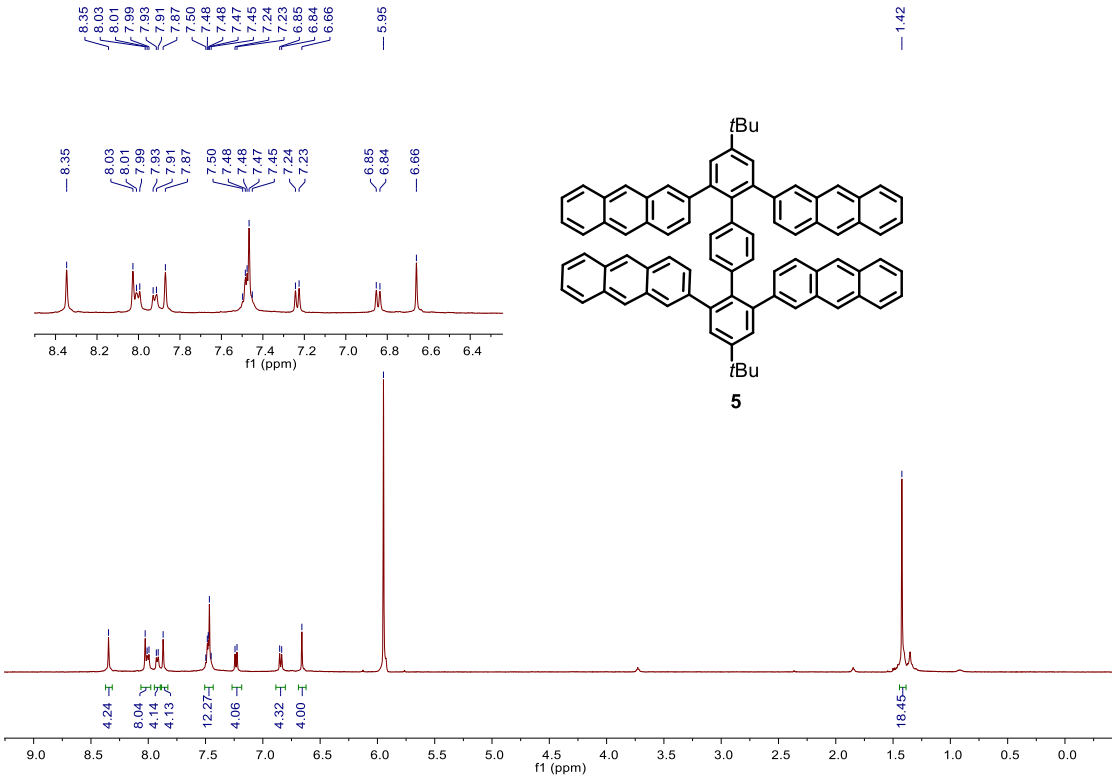

Figure S12. ^{1}H NMR spectrum of **5** (500 MHz, $C_2D_2Cl_4$, 413K).

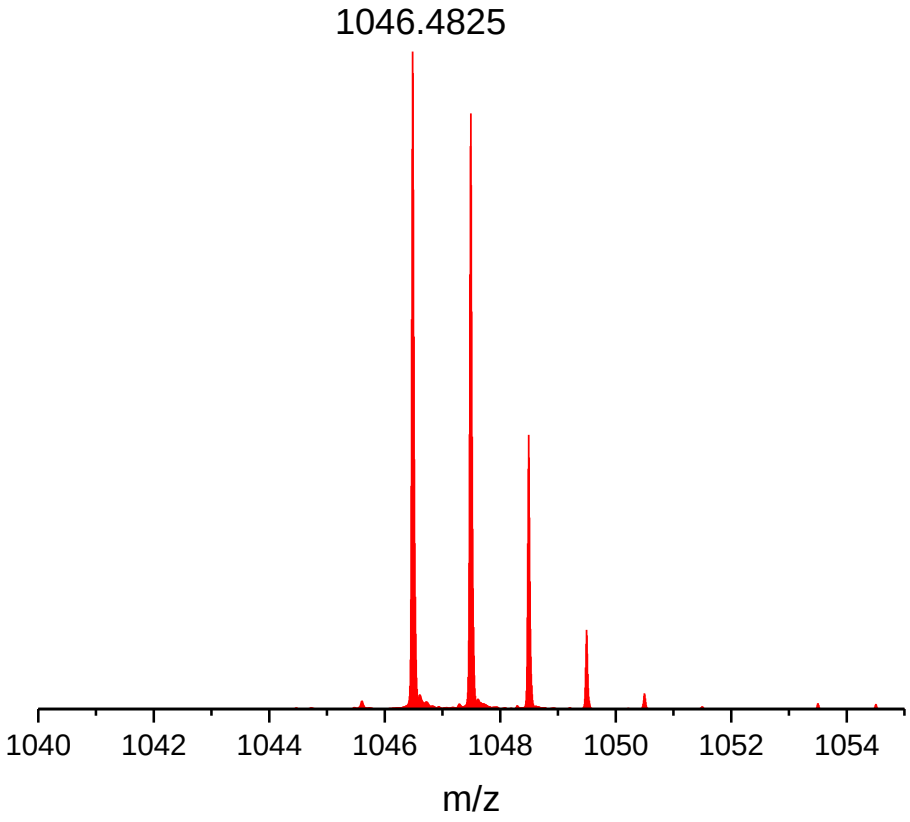

Figure S13. HRMS (MALDI-TOF) spectrum of **5**.

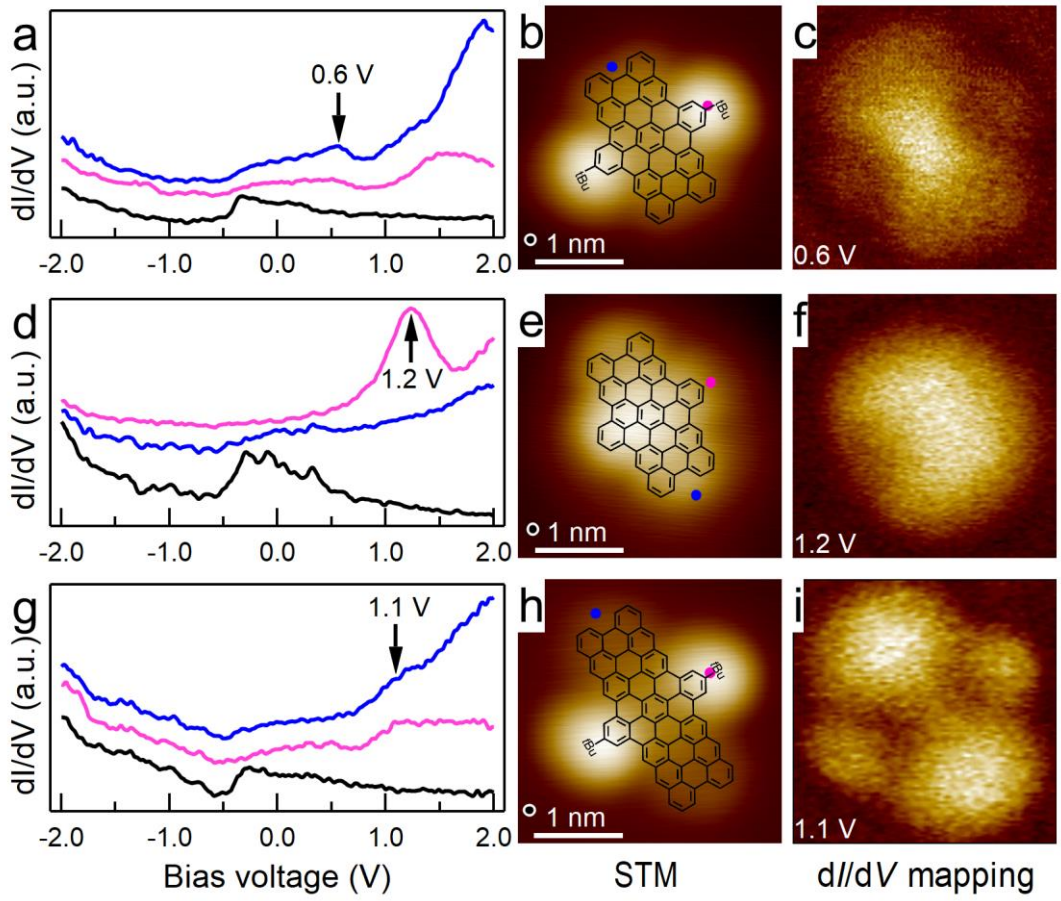

Figure S14. Electronic properties of dibenzoperihexacenes **3a** and **3b** (with and without *t*Bu groups) and dibenzoperioctacene **6** (with *t*Bu groups) measured on Cu(111). (a,d,g) STS spectroscopies recorded at the positions marked in the corresponding STM images (b,e,h) with the same colored dots. The spectra are vertically offset from each other for clarity. (b,e,h) STM images of individual nanographene molecules with the corresponding molecular structures overlaid (Imaging setpoint: (b,h) -1.0 V, 100 pA; (e) 0.1 V, 100 pA); and (c,f,i) 2D d*I*/d*V* maps recorded at 0.6 V, 1.2 V and 1.1 V, respectively.

References:

1. Hu, Y. B.; Wang, X. Y.; Peng, P. X.; Wang, X. C.; Cao, X. Y.; Feng, X. L.; Müllen, K.; Narita, A. *Angew. Chem. Int. Ed.* **2017**, *56*, 3374.
2. Dumslaff, T.; Yang, B.; Maghsoumi, A.; Velpula, G.; Mali, K. S.; Castiglioni, C.; De Feyter, S.; Tommasini, M.; Narita, A.; Feng, X. L.; Müllen, K. *J. Am. Chem. Soc.* **2016**, *138,* 4726.
3 Gaussian 09, Revision D.01, Frisch, M. J.; Trucks, G. W.; Schlegel, H. B.; Scuseria, G. E.; Robb, M. A.; Cheeseman, J. R.; Scalmani, G.; Barone, V.; Mennucci, B.; Petersson, G. A.; Nakatsuji, H.; Caricato, M.; Li, X.; Hratchian, H. P.; Izmaylov, A. F.; Bloino, J.; Zheng, G.; Sonnenberg, J. L.; Hada, M.; Ehara, M.; Toyota, K.; Fukuda, R.; Hasegawa, J.; Ishida, M.; Nakajima, T.; Honda, Y.; Kitao, O.; Nakai, H.; Vreven, T.; Montgomery, Jr., J. A.; Peralta, J. E.; Ogliaro, F.; Bearpark, M.; Heyd, J. J.; Brothers, E.; Kudin, K. N.; Staroverov, V. N.; Kobayashi, R.; Normand, J.; Raghavachari, K.; Rendell, A.; Burant, J. C.; Iyengar, S. S.; Tomasi, J.; Cossi, M.;Rega, N.; Millam, N. J.; Klene, M.; Knox, J. E.; Cross, J. B.; Bakken, V.; Adamo, C.; Jaramillo, J.; Gomperts, R.; Stratmann, R. E.; Yazyev, O.; Austin, A. J.; Cammi, R.; Pomelli, C.; Ochterski, J. W.; Martin, R. L.; Morokuma, K.; Zakrzewski, V. G.; Voth, G. A.; Salvador, P.; Dannenberg, J. J.; Dapprich, S.; Daniels, A. D.; Farkas, Ö.; Foresman, J. B.; Ortiz, J. V.; Cioslowski, J.; Fox, D. J. Gaussian, Inc., Wallingford CT, **2013**.